NASA TECHNICAL NOTE

ANALYTIC PERFORMANCE OF TWO-GRID ACCELERATOR DESIGNS FOR KAUFMAN THRUSTERS

by Walter C. Lathem

Lewis Research Center

Cleveland, Ohio 44135

1. Report No. NASA TN D-6275	2. Government Accession No.	3. Recipient. 0133062
4. Title and Subtitle ANALYTIC PERFORMANCE OF TWO-GRID ACCELERATOR DESIGNS FOR KAUFMAN THRUSTERS		5. Report Date April 1971
		6. Performing Organization Code
7. Author(s) Walter C. Lathem		8. Performing Organization Report No. E-6032
		10. Work Unit No. 120-26
9. Performing Organization Name and Address Lewis Research Center National Aeronautics and Space Administration Cleveland, Ohio 44135		11. Contract or Grant No.
		13. Type of Report and Period Covered Technical Note
12. Sponsoring Agency Name and Address National Aeronautics and Space Administration Washington, D. C. 20546		14. Sponsoring Agency Code

15. Supplementary Notes

16. Abstract

Results are presented for a theoretical analysis of the performance of two-grid accelerator systems for Kaufman thrusters. Six configurations were used to cover the range of geometries which are of immediate interest. A digital computer program was used to find axially symetric solutions for a single hole of each configuration. Results are presented in terms of maximum current per hole, thrust per hole (including beam divergence effects), and maximum net- to total-voltage ratio consistent with the prevention of electron backstreaming. The results presented herein should be useful in the design of accelerator systems for a variety of applications. An analysis of the effects of charge-exchange ions on the erosion rate of the accelerator grid resulted in equations which could be used to predict the expected useful lifetime of the grid. The equations seemed consistent when theoretical results were compared with experimental results for the SERT II configuration. However, when applied to the configurations used in this analysis, limitations in the usefulness of the model were found and are presented herein.

17. Key Words (Suggested by Author(s)) Electric propulsion Ion thruster Accelerator systems	18. Distribution Statement Unclassified - unlimited
19. Security Classif. (of this report) Unclassified	20. Security Classif. (of this page) Unclassified	21. No. of Pages 27	22. Price* $3.00

ANALYTIC PERFORMANCE OF TWO-GRID ACCELERATOR

DESIGNS FOR KAUFMAN THRUSTERS

by Walter C. Lathem

Lewis Research Center

SUMMARY

Results are presented for a theoretical analysis of the performance of two-grid ac-
celerator systems of Kaufman thrusters. Six configurations were used to cover the
range of geometries which are of immediate interest. A digital computer program was
used to find axially symetric solutions for a single hole of each configuration. Results
are presented in terms of maximum current per hole, thrust per hole (including beam di-
vergence effects) and maximum net- to total-voltage ratio consistent with the prevention
of electron backstreaming. The results presented herein should be useful in the design
of accelerator systems for a variety of applications.

An analysis of the effects of charge-exchange ions on the erosion rate of the accel-
erator grid resulted in equations which could be used to predict the expected useful life-
time of the grid. The equations seemed consistent when theoretical results were com-
pared with experimental results for the SERT II configuration. However, when applied
to the configurations used in this analysis, limitations in the usefulness of the model were
found and are presented herein.

INTRODUCTION

Accelerator systems used to extract mercury ions from the plasma discharge of
Kaufman thrusters and exhaust them at high velocity have typically been designed by em-
pirical techniques. Performance trends were noted during experimental tests at Lewis
Research Center over a period of years, and design "rules of thumb" were established
(refs. 1 to 3). Since this early work, various analog and digital computer techniques
(refs. 4 to 7) have become available. More recently a theoretical analysis of the effects
of varying the geometrical and electrical parameters of a two-grid accelerator system
was made (ref. 8). The results initially reported in reference 8 are discussed herein in
greater detail. In addition, the results of the charge-exchange ion erosion portion of this
analysis are correlated with experimental erosion results for a 1000-hour life test of a

SERT II accelerator grid system (ref. 9). SERT stands for Space Electric Rocket Test. The SERT II mission is an orbital test of a 15-centimeter-diameter Kaufman thruster. The SERT II vehicle was launched on February 2, 1970.

The analysis reported herein utilizes a more detailed description of the shape and location of the downstream plasma boundary and ion impingement patterns on the accelerator grid than has been previously reported.

MODEL

Figure 1 is a cutaway view of a typical two-grid accelerator system showing the single hole model. The holes in this grid set are match drilled, with the simple untapered holes arranged in a hexagonal array. Figure 2 identifies the geometric variables needed to define the accelerator system. The webbing thickness w_a represents the minimum distance between two immediately adjacent holes (see insert, fig. 2).

For the comparison with experimental SERT II erosion results, the observed erosion pattern should also be described. During thruster operation, charge-exchange ions can be formed in the beam region by a transfer of charge between fast-moving beam ions and slow-moving neutral atoms which have escaped the discharge chamber. These newly formed slow ions are attracted by the negative potential of the accelerator grid. When they impinge, metal atoms are sputtered from the grid. Figure 3 shows the resulting erosion in the form of a hexagonal-shaped pattern around each grid hole on a grid which was operated for about 800 hours. The erosion channel depth is a minimum at points midway between immediately adjacent holes (point a) and maximum at center points of three adjacent holes (point B). Obviously, when the channel has been eroded through at point A, the hexagonal section of grid around the hole will separate from the rest of the grid. This section could lodge between grids, which would short out the accelerator system and cause an immediate end to the usefulness of the grid system. Even if the section of grid separated without causing such problems, the loss of the section would reduce the ion extraction capability of the accelerator system. For subsequent calculation, the useful lifetime (on a single-hole basis) is assumed to be the time required for charge-exchange ions to erode through the accelerator grid at point A.

GENERAL APPROACH

There are obviously many possible configurations involving variations in the geometric parameters shown in figure 2. Figure 4 shows a few representative configurations which were selected to allow interpolation of results to many other configurations. Configurations 1, 2, 4, 5 and 6 are labeled to indicate how they differ from configuration 3

which was chosen as the basic configuration because in general it is similar to accelerator systems presently in use (on SERT II, for example). Numerical values for configuration 3 geometrical and electrical parameters are given in table I. Typical variations in five of the variables are described in figure 4 and compared in the included table. The screen hole diameter d_s was held fixed. In addition, the screen grid thickness t_s was held fixed because of limitations involved in using the digital computer program. The reason becomes clear upon examination of figure 5. Although the screen thickness in figure 5(b) is twice that in figure 5(a) the discharge chamber plasma boundary in both cases is such that the bounded regions which must be defined for the computer program are identical. In effect, the screen electrode can extend any depth into the plasma without affecting the results of the computer program. In practice, of course, the thicker screen of figure 5(b) would lead to more ions recombining on the screen, and poorer overall thruster performance.

A total of 17 different cases, including variations in accelerator grid voltages, beam current levels, and geometric variables were analyzed using a digital computer program (ref. 4) which yielded, as part of the output, the beam current and the thrust per hole. From these results, values for the maximum current per hole (at constant grid voltage) were obtained for each configuration.

In addition to these cases, the SERT II accelerator grid system was analyzed to correlate theoretical results with experimental test results and to estimate the expected accelerator grid lifetime.

METHOD OF SOLUTION

The digital computer program (ref. 4) was used to obtain the space-charge-limited current and the thrust for each configuration. Computer solutions can be obtained for almost any configuration exhibiting axial symmetry. To obtain alternate solutions for a given geometric configuration, it is only necessary to assign a value of beam current and then vary the shape and location of the plasma sheath until the current density is uniform across the sheath and the assigned value of beam current is obtained. Each solution yields a different total current per hole depending on the sheath positions and the voltages applied to the grids. During actual thruster operation, the level of this current is controlled by the ion density in the discharge chamber plasma.

The shape and location of the boundary which separates the ion beam from the neutralized downstream plasma can be varied considerably without significant effect on the computed total beam current or ion trajectories. However, as pointed out in reference 6, the location and shape of this boundary are important for explaining the accelerator grid erosion patterns caused by charge-exchange ions in experimental thrusters. Various downstream plasma boundaries are shown in figure 6. (This figure is a cross

section passing through point A of fig. 3.) When a flat downstream boundary was set up for this model in the electrolytic tank analog (ref. 5) and ion trajectories plotted, very few trajectories terminated at point A, even though in the plane of this cross section the majority of accelerator grid erosion is observed from experiment to occur at this location. Consideration of ion space-charge effects indicates that the boundary would be contoured as shown by the heavy line in figure 6, and in figure 7. When a contoured downstream boundary was used in the analysis, most of the charge-exchange ion trajectories from the downstream plasma were focused into the center of the webbing, thus giving an impingement pattern in agreement with experimental observations.

To determine the proper location and shape of the downstream boundary, the following method was used: Three digital computer solutions were obtained for the same configuration, each with a different trial downstream boundary (straight solid lines in fig. 6 labeled 1, 2, and 3). These different downstream boundaries resulted in essentially no changes in the primary ion beam trajectories and only a slight change in the total current extracted for each configuration. The trial boundaries were all set at ground potential (assuming the neutralized downstream plasma potential was zero). In each case an additional zero-voltage line (curved solid lines labeled 1', 2', and 3' in fig. 6) appeared in the computer solution. The region between the trial boundary zero line and the corresponding primed zero line was at positive potential. The greater the distance between these lines, the higher the positive potential was between them. As the trial boundary and corresponding primed zero lines approach one another in subsequent solutions, the top portion of the primed line merges with the beam bounding ion trajectory (dashed line). The final boundary used in subsequent calculations is shown in figures 6 and 7 as a heavy solid line (labeled 4 in fig. 6). This boundary is shown departing from the beam bounding ion trajectory near the top of figures 6 and 7 because it is believed that in practice there are no sharp changes in contour in the plasma boundary. A few charge-exchange ions outside of the beam, for example, would result in a contour similar to that shown.

For discussion purposes, the accelerator electrode is divided into erosion regions 1 and 2 shown in figure 7. The ion beam is divided into regions A, B, and C in this figure. When cases were run on the electrolytic tank analog, it was observed that charge-exchange ions originating within region B and partway within region C arrive at region 1 of the accelerator. Charge-exchange ions originating in the portion of region C near the beam edge arrive at region 2 of the accelerator. Charge-exchange ions originating in region A escape the thruster. In figure 7, the size of erosion region 1 has been exaggerated for clarity. Results of many experiments have shown the erosion to be much less in region 1 than in region 2 for geometries similar to SERT II.

RESULTS AND DISCUSSION

The results are presented in the following order: The results of the digital computer analysis of the general configurations in terms of ion beam optics and electron back-streaming limits are stated. An analytical model used to estimate the grid lifetime for the SERT II configuration is then discussed. Finally, some limitations of the model when applied to other configurations are presented.

General Configuration Results

Ion beam optics. - Results of the digital computer analysis for the 17 cases considered are presented in table II. The screen voltage (net accelerating voltage) was 1600 volts for these cases. As indicated in column 2 of table II, the negative voltage was -400 volts for all cases except 2a and 3a, where the voltage was -1067 volts. Geometrically, configurations 2a and 3a were identical to configurations 2 and 3, respectively (see fig. 4). Values of ion beam current per hole are shown in column 3. In several cases a range of beam currents was considered for the same electrode geometry. This required separate solutions for the shape and location of the upstream plasma sheath for each different beam current. For cases 2a and 3a, each of the beam currents was obtained by first obtaining sheath solutions for cases 2 and 3 and then changing only the negative accelerator voltage. For example, the sheath shape and location which yielded 0.41 milliamperes in configuration 2 yields 0.63 milliamperes when the voltage is changed to -1067 volts (configuration 2a). This result reflects the 3/2 power relation to the voltage, as would be expected from the Child's law relation.

Corresponding thrust values are shown in column 4 and thrust coefficients in column 5. The thrust coefficients were obtained by dividing the total thrust from the computer program (which corrects for beam divergence) by the theoretical value obtained by assuming zero divergence. The computer program computes the thrust using the axial component of velocity for each stream tube of current as it crosses the downstream plasma sheath. In some cases (those footnoted in column 5 of table II), a portion of the beam is intercepted by the accelerator or by the upper boundary of the region of interest before reaching the downstream boundary. This occurs with highly divergent beams. That portion of the beam is not included in the total thrust value given by the computer for such configurations. Therefore, for the footnoted cases the thrust values in column 4 were hand calculated using the ion velocity value given by the computer program at the point of interception with the upper boundary. Ions striking the accelerator were not included in any case. Even though these velocity values would not be much different than values expected at the downstream boundary, the resulting thrust values were not deemed accurate enough to yield meaningful thrust coefficients. For example, the ions are

decelerating in this region and the hand-calculated value using the last-known velocities yields a thrust coefficient greater than unity for at least one case. Table II shows that for similar beam current levels, all configurations yield approximately the same thrust. This is because the thrust coefficients are all near unity.

Columns 6, 7, and 8 of table II present the data used to determine the maximum allowable current per hole values shown in the last column. In that regard, figure 8 indicates the effect of beam current variations on the plasma sheath location and the bounding ion trajectory for a typical configuration. As the beam current per hole increases, the sheath moves downstream (while becoming flatter) and the ion beam radius increases. By definition herein, the upper limit of beam current is reached when the maximum value of the beam diameter (within the bounds of the accelerator) is equal to the accelerator hole diameter (i. e., when the ratio of beam diameter to accelerator hole diameter equals unity). Columns 6, 7, and 8 of table II summarize the values of maximum beam diameters, accelerator hole diameters, and the corresponding ratios for the various configurations. The beam current per hole values from column 3 are plotted in figure 9 against ratios of maximum beam diameter to accelerator hole diameter from column 8.

An extrapolation was used in some cases to reach the line where the ratio was unity (vertical dashed line in fig. 9). Values of the maximum allowable current per hole for each configuration were read from this plot at the points of interception of the curves with the dashed line and tabulated in column 9 of table II. The maximum current per hole values for configurations 2a and 3a were also found by the method of figure 9 and, in addition, were checked by calculating them from the values given for configurations 2 and 3 and using a 3/2 power relation of the change in voltage.

It is of interest to compare the results of configurations 3 and 4, where, as noted in figure 4, the only change is in the grid spacing y (i. e., $y_4 = 2y_3$). For a one-dimensional, space-charge-limited flow model, the current scales as the inverse square of the acceleration distance. If the centerline-to-centerline grid spacing $((t_s/2) + y + (t_a/2))$ is used for the acceleration distance, the current-per-hole ratio for configurations 3 and 4 is given by

$$\frac{J_{h,4}}{J_{h,3}} = \frac{\left(\dfrac{t_s}{2} + y + \dfrac{t_a}{2}\right)^2}{\left(\dfrac{t_s}{2} + 2y + \dfrac{t_a}{2}\right)^2} \tag{1}$$

(All symbols are defined in appendix A.) From equation (1) a value of 0.17 was calculated for the maximum current per hole of configuration 4. This value compares favorably with the value of 0.16 given in table II, column 9. This acceleration distance also has been used in another analysis (ref. 1) to estimate the fraction of Child's law flow in

6

ion thrusters. The present analysis further supports the idea of using the distance $((t_s/2) + y + (t_a/2))$ as a meaningful ion thruster grid design parameter.

Electron backstreaming limits. - In determining operating grid voltages for an ion thruster it is useful to be able to predict how close to zero-voltage the accelerator potential can be set without allowing electrons from the neutralizer to be accelerated back through the grid system. By analyzing various net- to total-voltage ratios using the digital computer and examining the resulting interelectrode potential distributions, it is not difficult to determine the maximum allowable net- to total-voltage ratio above which there would be no negative barrier to the backstreaming electrons. Computer results for the SERT II case were examined and a maximum allowable voltage ratio of 0.95 was determined. In experimental tests, backstreaming was observed to occur within a few percent of this ratio.

Table III summarizes the results for the configurations studied by giving the total voltages applied (column 2) and the maximum allowable ratio of net- to total-voltage R_{max} (column 3). The data show that the ratio R_{max} is configuration dependent rather than voltage dependent. Values for beam current per hole also are listed in table III to show that, for the range of currents analyzed, the actual level of current has little effect on the ratio R_{max}. In addition, the screen voltages obtained by multiplying the total voltages by the corresponding voltage ratios indicate the upper limit to the useful range of specific impulse. For example, for a total voltage of 2000 volts, configuration 5 allows a maximum specific impulse of about 4400 seconds, while the maximum for configuration 2 is about 4100 seconds (assuming 100-percent propellant utilization for both).

Special Case: SERT II Accelerator System

Several elements need to be considered in arriving at an estimate of accelerator grid lifetime. For example, determination of the shape and location of the downstream plasma sheath and a definition of the charge-exchange-ion extraction volumes are necessary in constructing the analytical model. These elements are discussed in the following paragraphs.

Downstream boundary. - Using the method described earlier, the downstream boundary (zero potential) was established for a single-hole model of the SERT II accelerator system. The model represented a hole near the center of the grid where the beam current per hole is found experimentally to be about 0.6 milliampere. According to the results of the analysis, the downstream boundary is nonplanar, being closer to the accelerator at the center of a hole than at the center of the webbing between the holes. The boundary, illustrated qualitatively in figure 10, also shows the boundary to be closer to A-type points than to B-type points. In figure 10, the horizontal plane which represents a cross section through a single row of holes intercepts only A-type points. In the

vertical plane, the cross section cuts through both A- and B-type points. The shape of the downstream plasma boundary in the vertical plane indicates that charge-exchange ions accelerated from the plasma to the accelerator would be focused toward the B-type points. In both planes, the shapes indicate a focusing toward the center of the webbing.

For the SERT II analytical model, the distance to the downstream plasma boundary where the ion beams intersect at a point (which was assumed to be at zero volts) was estimated by using the digital computer program to be about 13.0 millimeters. Probe measurements reported in reference 10 indicated that the beam potential was about 40 volts at a distance of 12.7 millimeters from the accelerator. This 40-volt difference between theory and experiment is a small fraction of the 2000-volt difference between the accelerator and the boundary. Thus, the apparent agreement between the boundary location predicted by the analysis and the location found by experimental measurement lends credence to the analytical method used herein for establishing the downstream plasma boundary.

Charge-exchange-ion extraction volume. - Charge-exchange ions responsible for the erosion of region 2 of the accelerator were found to originate in the portion of region C near the ion beam boundary (fig. 7). The volume of this portion of region C consists of a surface area A_c which is formed by the intersection of three conical-shaped beams, and a thickness d_c. Although it is difficult to illustrate the area by way of a figure, the calculation is straightforward. Details of the calculation are given in appendix B. The following formula was used to calculate the thickness d_c for the SERT II configuration:

$$d_c = \frac{V_2}{SA_c Q \mu^+ \rho^0 \tau}$$

(2)

where

A_c area of plasma boundary coincident with beam boundary, m^2

Q cross section for charge-exchange interaction, m^2

S volume sputtering rate of accelerator material, m^3/ion

V_2 volume of material sputtered from region 2 of the accelerator, m^3

μ^+ primary beam ion flux, ions/(m^2)(sec)

ρ^0 neutral atom density, atoms/m^3

τ total thruster operating time, sec

The following procedure was used in applying this formula to the SERT II configuration: Surface analysis of a SERT II grid which had been tested in a vacuum facility for 1000 hours yielded erosion pit (point B) profiles like those shown in figure 11. The depth of

8

the pits varied with radial position on the grid, with the deepest being at the center of the grid. A typical pit near the center of the grid was about 0.38 millimeter deep and had a 45° half angle. Since the pits were approximately conical, the volume V_2 was calculated on this basis for the deepest pit. The result was $V_2 = 8.5 \times 10^{-11}$ cubic meters.

The sputtering rate, $S = 4 \times 10^{-29}$ cubic meters, was taken from references 11 and 12 using 2000-volt charge-exchange ions with normal incidence. The area, $A_c = 4.47 \times 10^{-5}$ square meters, was calculated by the method of appendix B. The cross section, $Q = 6.4 \times 10^{-19}$ square meters, was obtained from reference 13 for 3000-volt primary beam ions. The primary ion flux, $\mu^+ = 2.35 \times 10^{20}$ ions per square meter per second, was obtained by dividing the beam current (6×10^{-4} A) by the cross-sectional area of the beam (1.58×10^{-5} m^2) in the region near the downstream plasma. The neutral density, $\rho^O = 7.9 \times 10^{17}$ atoms per cubic meter, was obtained from the equation

$$\rho^O = \frac{1}{1.6 \times 10^{-19}} \frac{J_o}{\dfrac{A_B \overline{v}}{4}} \tag{3}$$

where J_o is the neutral atom flow in equivalent amperes based on a beam current of 6×10^{-4} amperes and a propellant utilization efficiency of 85 percent, A_B is the cross-sectional area of the beam at the downstream boundary (1.58×10^{-5} m^2), and $\overline{v}$ is the neutral atom velocity from

$$\overline{v} = \left(\frac{2kT}{m}\right)^{1/2} \tag{4}$$

In equation (4), a temperature of 700 K was used. Finally, the time τ was 3.6×10^6 seconds (1000 hr). Substitution of all these values in equation (2) yields a thickness d_c of 0.11 millimeters.

This distance seems reasonable when compared to the Debye shielding distance for this region of the downstream plasma. The Debye shielding distance is given by

$$\lambda_D = 7.43 \times 10^6 \left(\frac{T_e}{\rho_i}\right)^{1/2} \quad \text{millimeters} \tag{5}$$

where T_e is the electron temperature in eV; and ρ_i is the ion density in ions per cubic meter which can be obtained from

$$\rho_i = \frac{\mu^+}{(2\eta V_s)^{1/2}} \tag{6}$$

9

where μ^+ has already been given, η is the charge-to-mass ratio of singly charged mercury ions $(4.8 \times 10^5$ C/kg), and V_s is the net accelerating voltage (3 kV). If the average electron temperature is assumed to be 1 eV, the result of equation (5) is $\lambda_D = 0.11$ millimeter, which agrees with the resulting thickness d_c previously calculated. It was concluded then that the charge-exchange ions that are responsible for the erosion of the accelerator in region 2 are formed in a volume which can be defined by the portion of the boundary of region C coincident with the bounding ion beam trajectory and a thickness equal to the Debye shielding distance at that point.

Theoretical grid lifetime. - As previously discussed, the useful lifetime of a particular grid for ion extraction is based on the erosion at the minimum erosion channel depth (point A in fig. 10). For the 1.5-millimeter-thick SERT II grid, the depth at this point was approximately 7 to 10 percent of the depth at the maximum erosion point, point B (which was 0.38 mm for the deepest pit). Typical erosion depth for an A-type point was about 0.033 millimeter. A cross section of the erosion channel at point A shows a V-shaped groove (fig. 12). The groove half-angle is defined as α. All ions impinging on region 2 are assumed to arrive normal to the plane of the accelerator, and therefore the angle of incidence is defined in figure 12 as β (the angle between the ion trajectory and a normal to the surface of the groove). It is seen that α is equal to $90^{\circ} - \beta$.

If atoms sputtered from the surface of such a groove are assumed to leave the surface with a cosine distribution, some of the substrate atoms will redeposit on the opposite walls and effectively reduce the sputtering yield or erosion rate. In fact, if the impinging ions are uniformly distributed across the groove, the amount of material which escapes is proportional to sin α and an effective sputtering yield can be defined as

$$S_{eff} = S \times \sin \alpha = S \times \sin(90^{\circ} - \beta) \tag{7}$$

Data from references 11 and 12 which show the sputtering rate as a function of the angle of incidence β for angles between 0° and 60° were used in conjunction with equation (7) to obtain effective sputtering rates for the SERT II case. Results showed that for 2000-volt ions, the effective sputtering rate is nearly constant for this range of β. For lack of data, it was assumed that the effective sputtering rate would remain constant for angles greater than 60°. Data for ions and materials other than mercury and molybdenum indicate a peak in the sputtering rate at about 65° to 70°, making this possibly a conservative estimate.

The preceding discussion indicates that even though the erosion-groove geometry changes with time, the effective sputtering rate is approximately linear with time. Data from tests of a cesium bombardment engine (ref. 14) indicated that the erosion rate decreased with time rather than being linear. Therefore a conservative estimate of the useful lifetime of the SERT II grid can be obtained by a linear extrapolation of the 1000-hour data. The result is a lifetime estimate of about 46 000 hours. This estimate, of course,

10

is for the main region of the accelerator and does not include any localized effects such as are known to exist in the vicinity of the neutralizer.

It should be noted that the grid analyzed here was tested in a 1.5-meter-diameter by 1.8-meter-long vacuum facility with the beam directed into a frozen mercury target. Additional mercury atoms would arrive from the target at the accelerator region so that the erosion rate would be lower in a space flight in the absence of such a target.

Limitations of Analytical Model

If the model used to estimate the grid lifetime for the SERT II were completely general, it could be applied to the configurations discussed earlier in this paper. For example, equation (2) could be rewritten in terms of the thruster running time τ; that is,

$$\tau = \frac{V_2}{d_c A_c S Q \mu^+ \rho^0} \tag{8}$$

To apply this equation to the erosion at point A so that a lifetime estimate can be obtained, the volume V_2 must be defined in terms of the depth of erosion h at point A and the downstream plasma surface area A_c must also be defined. The remaining parameters in equation (8) are readily defined in terms of the particular configuration geometry and voltages.

When an attempt was made to apply the model to all the general configurations, some limitations became readily apparent:

(1) The definition of the downstream plasma surface given earlier cannot be applied to a configuration in which adjacent ion beams diverge very slowly; that is, a small divergence angle leads to near-infinite plasma boundary surface areas if the method of appendix B is used. Also, unreasonably high estimates for the distance from the accelerator to the downstream plasma sheath are obtained. In this type of configuration the zero potential line cannot be expected to follow the bounding beam trajectory. Additional information is required concerning the detailed behavior of the potential field lines in this region. Examples of configurations exhibiting these low divergence angles are the low-current cases of configurations 2, 2a, 3, 3a, and 4 (see table II).

(2) A problem arises also for beams with very high divergence angles. In this case the trajectories of adjacent beams intersect upstream of the zero potential line and the plasma boundary surface area as defined in appendix B approaches zero. An infinite-lifetime prediction would result from application of the model to this type of configuration. Erosion on the sides of the holes would also become more important. Examples are the high current cases of configurations 2, 2a, 3, and 3a.

(3) A third limitation arises from the inability to predict the erosion volume V_2. Without prior knowledge of the erosion-groove dimensions, a calculation is needed which involves, among other things, the energy, angle of incidence and distribution of the impinging ions. Obtaining this information requires accurate plotting of charge-exchange-ion trajectories starting from the downstream plasma. To date, this has not been possible because of physical limitations in the electrolytic tank analog and storage limitations in the digital computer program.

It is clear then that a better understanding of the behavior of the downstream plasma sheath is needed. The main drawback to the model presented herein appears to lie with the determination of the plasma boundary for both high- and low-current configurations and the extensive analysis required to predict the charge-exchange erosion volume.

CONCLUDING REMARKS

The effects of varying the geometrical and electrical parameters of a two-grid ion accelerator system have been presented in terms of ion beam optics. The parameters involved included
(1) Screen and accelerator grid thicknesses
(2) Screen and accelerator hole diameters
(3) Grid separation distance
(4) Grid fraction open area
(5) Grid voltages
(6) Ratio of grid voltages
(7) Sheath shapes and location
A number of representative cases were studied which cover a wide range of variables. Additional results can be obtained by scaling and interpolation of the results given.

A SERT II grid was examined for experimental erosion data and an extrapolated lifetime calculated. Limitations were discussed in conjunction with the application of the model used in the SERT II calculation. It was concluded that additional information is still needed to obtain useful lifetime predictions that can be generalized.

Other results of the analysis include the prediction of the accelerator potential needed to prevent electron backstreaming, the definition of a specific impulse range for each configuration and each value of total voltage, and a digital computer technique for locating the position and approximate shape of the downstream plasma boundary.

Lewis Research Center,
    National Aeronautics and Space Administration,
        Cleveland, Ohio, December 28, 1970,
            120-26.

APPENDIX A

SYMBOLS

A_B cross-sectional area of beam at downstream boundary, m^2

A_c surface area of charge-exchange-ion extraction volume, m^2

A_F surface area of frustrum of cone (see appendix B)

A_I surface area of ion beam intersection region (see appendix B)

d_a accelerator hole diameter, m

d_B maximum single-hole ion beam diameter measured within plane of accelerator grid, m

d_c thickness of charge-exchange-ion extraction volume, m

d_s screen hole diameter, m

h depth of erosion of region 2 at middle of accelerator grid webbing, m

J_h beam current per hole, mA

J_o neutral atom flux, equivalent mA

Q charge-exchange cross section, m^2

R ratio of screen voltage to total accelerating voltage

r radius of ion beam

S sputtering rate of accelerator grid, m^3/ion

t_a accelerator grid thickness, m

t_s screen grid thickness, m

V_a screen voltage, V

V_2 volume of material sputtered from region 2 of accelerator, m^3

$\bar{v}$ neutral atom velocity, m/sec

w_a thickness of webbing between adjacent holes in accelerator grid, m

w_s thickness of webbing between adjacent holes in screen grid, m

y grid separation distance, m

α erosion-groove half-angle

β incidence angle of impinging ion

η charge-to-mass ratio of singly ionized mercury

θ ion beam divergence angle

μ^+ primary beam ion flux, ion/(m^2)(sec)

$\dot{\mu}$ arrival rate density of charge-exchange ions at middle of webbing, ion/(m^2)(sec)

ρ^o neutral atom density, atoms/m^3

τ thruster operating time, sec

APPENDIX B

SURFACE AREA OF DOWNSTREAM PLASMA BOUNDARY

To calculate the thickness of the downstream charge-exchange-ion extraction volume for the SERT II configuration and to compare the resulting value with the calculated Debye shielding distance for this region, an accurate determination of the surface area of the plasma boundary was required. The value used for the area A_c in equation (2) was obtained by the following method.

The region of interest is that portion of the plasma boundary immediately downstream of the deepest erosion point between three accelerator holes (point B, fig. 3). Figure 10 shows a cross-section view of the plasma boundary. A more complete description of the boundary is given in figure 13. In figure 13, three diverging ion beams are shown intersecting each other downstream of the accelerator grid. A 7° divergence angle, obtained from the digital computer program, was used for the calculation. The plasma boundary can be divided into three distinct zones, two of which are related to the erosion of the accelerator at point B. The zones are identified in the following paragraphs (refer to fig. 13).

Zone 1 is the area of the circle at position 1. It is entirely within the ion beam and is the closest portion of the plasma boundary to the accelerator grid. Charge-exchange ions formed in zone 1 do not contribute to erosion at point B.

Zone 2 is the surface of the frustrum of the cone between position 1 and position 2. Position 2 is the axial location where the ion beams first intersect each other. Charge-exchange ions formed in the beam near the surface of this zone do contribute to erosion at point B. The surface area of the frustrum was calculated from the equation

$$A_F = \frac{\pi\left(r_2^2 - r_1^2\right)}{\sin \theta} \tag{B1}$$

where

r_2 radius of beam at position 2

r_1 radius of beam at position 1

θ ion beam divergence half-angle

From the digital computer results, $r_2 = 2.25$ millimeters, $r_1 = 1.4$ millimeters, and $\theta = 7^O$. From equation (B1) the area of the frustrum of the cone for this case is 80.0 square millimeters.

Zone 3 is the most difficult to visualize. It is the region where the three ion beams overlap. Each of the three sides of the pyramid-shaped region shown in figure 13 is associated with one of the three cones. The heavy lines in figure 13 are the locus of points formed by the intersection of each pair of cones. The lines come to a point where all three cones intersect. The surface area of zone 3 can be obtained from the equation

$$A_I = 0.162 \frac{r_2^2}{\sin \theta} \tag{B2}$$

where r_2 and θ have been previously defined. The result for the SERT II case is $A_I = 6.7$ square millimeters.

All of the zone 3 area A_I contributes charge-exchange ions that can arrive at point B, however, only one-sixth of the zone 2 area A_F of each of the three beams contributes at that point; that is,

$$A_c = A_I + 3\left(\frac{A_F}{6}\right) \tag{B3}$$

or, for the case considered,

$$A_c = 46.7 \text{ square millimeters} \tag{B4}$$

This value was used in equation (2) to obtain the result for the plasma thickness d_c.

16

REFERENCES

1. Kerslake, William R.: Accelerator Grid Tests on an Electron-Bombardment Ion Rocket. NASA TN D-1168, 1962.

2. Kerslake, William R.; and Pawlik, Eugene V.: Additional Studies of Screen and Accelerator Grids for Electron-Bombardment Ion Thrustors. NASA TN D-1411, 1963.

3. Kaufman, Harold R.: Performance Correlation for Electron-Bombardment Ion Sources. NASA TN D-3041, 1965.

4. Bogart, Carl D.; and Richley, Edward A.: A Space-Charge-Flow Computer Program. NASA TN D-3394, 1966.

5. Staggs, John F.: An Electrolytic Tank Analog for Two-Dimensional Analysis of Electrostatic-Thrustor Optics. NASA TN D-2803, 1965.

6. Pawlik, Eugene V.; Margosian, Paul M.; and Staggs, John F.: A Technique for Obtaining Plasma-Sheath Configurations and Ion Optics for an Electron-Bombardment Ion Thrustor. NASA TN D-2804, 1965.

7. Lathem, Walter C.: A New Technique for Similating Space-Charge Potential Distributions. J. Spacecraft Rockets, vol. 5, no. 6, June 1968, pp. 737-738.

8. Lathem, Walter C.: Ion Accelerator Designs for Kaufman Thrusters. J. Spacecraft Rockets, vol. 6, no. 11, Nov. 1969, pp. 1237-1242.

9. Byers, David C.; and Staggs, John F.: SERT II: Thruster System Ground Testing. J. Spacecraft Rockets, vol. 7, no. 1, Jan. 1970, pp. 7-14.

10. Rawlin, Vincent K.; and Kerslake, William R.: SERT II - Durability of the Hollow Cathode and Future Applications of Hollow Cathodes. J. Spacecraft Rockets, vol. 7, no. 1, Jan. 1970, pp. 14-20.

11. Magnuson, G. D.: Sputtering Mechanisms Under Ion Propulsion Conditions. Rep. AE62-9517, General Dynamics Corp., May 10, 1962.

12. Cheney, K. B.; Rogers, E. E.; and Pitkin, E. T.: Research on Experimental Evaluation of Sputtering Yield Rates. Marquardt Corp. (ARL-63-125), July 1963.

13. Brown, Sanborn C.: Basic Data of Plasma Physics. Technology Press of MIT, 1959, p. 38.

14. Sohl, G.; Reid, G. C.; Barcatta, F. A.; Zafran, S.; and Speiser, R. C.: Ion Rocket System Research and Development. Rept. 4920-Final, Electro-Optical Systems, Inc. (NASA CR-54323), Dec. 30, 1965.

TABLE I. - NUMERICAL VALUES OF CONFIGURATION

3 PARAMETERS (SEE FIG. 4)

Screen hole diameter, d_s, mm	2.0
Screen thickness, t_s, mm	0.5
Grid separation, y, mm	1.0
Accelerator hole diameter, d_a, mm	1.33
Accelerator thickness, t_a, mm	1.0
Screen webbing thickness, w_s, mm	0.2
Accelerator webbing thickness, w_a, mm	0.87
Screen fraction open area, f_s	0.75
Screen voltage, V_s, volt	1600
Accelerator voltage, V_a, volt	-400
Net- to total-voltage ratio, R	0.8
Maximum beam current per hole, $J_{h, max}$, mA	0.42

[Screen voltage, 1600 V in each case.]

Configuration number (see fig. 4)	Accelerator voltage, V_a, V	Ion beam current per hole, J_h, mA	Thrust, μN	Thrust coefficient	Maximum beam diameter inside accelerator hole, d_B, mm	Accelerator hole diameter, d_a, mm	Ratio of maximum beam diameter to accelerator diameter, d_B/d_a	Maximum current per hole, $J_{h,max}$, mA (see fig. 9)
1	-400	0.29	23.6	0.993	1.07	1.33	0.81	~0.45
2	-400	0.41	33.5	(a)	1.77	2.00	0.89	0.52
		.29	23.6	0.989	1.36	2.00	.68	.52
		.17	13.8	.998	.77	2.00	.39	.52
2a	-1067	0.63	51.4	(a)	1.78	2.00	0.89	0.80
		.45	36.3	(a)	1.38	2.00	.69	.80
		.26	21.2	0.996	.77	2.00	.39	.80
3	-400	0.45	32.0	(a)	1.36	1.33	1.02	0.42
		.29	23.7	0.992	1.12	1.33	.85	.42
		.16	13.3	.999	.63	1.33	.47	.42
3a	-1067	0.69	50.3	(a)	1.36	1.33	1.02	0.65
		.45	20.4	0.986	1.13	1.33	.85	.65
		.25	20.4	.993	.63	1.33	.47	.65
4	-400	0.18	11.7	(a)	1.46	1.33	1.10	0.16
		.11	8.6	0.998	1.07	1.33	.81	.16
5	-400	0.29	23.6	0.989	1.28	1.33	0.96	~0.33
6	-400	0.25	20.5	0.993	1.08	1.33	0.81	~0.37

[a]Accurate total thrusts not available from computer results (see text). Thrust values of column 4 for these cases were hand calculated using extrapolated values of ion velocity.

TABLE III. - MAXIMUM ALLOWABLE NET- TO

TOTAL-VOLTAGE RATIO AS LIMITED

BY ELECTRON BACKSTREAMING

Configuration number (see fig. 4)	Total voltage, V	Maximum net- to total- voltage ratio, R_{max}	Beam current per hole, J_h, mA
1	2000	0.89	0.29
2	2000	0.87	0.41
		.87	.29
		.88	.17
2a	2667	0.84	0.63
		.85	.45
		.86	.26
3	2000	0.94	0.45
		.94	.29
		.94	.16
3a	2667	0.93	0.69
		.93	.45
		.93	.25
4	2000	0.97	0.18
		.97	.11
5	2000	0.99	0.29
6	2000	0.95	0.25
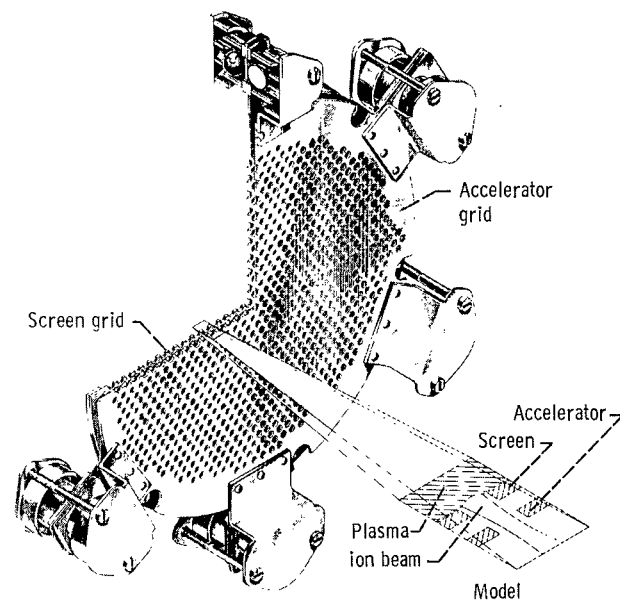
CD-9455

Figure 1. - Typical two-grid system showing the single-hole model.
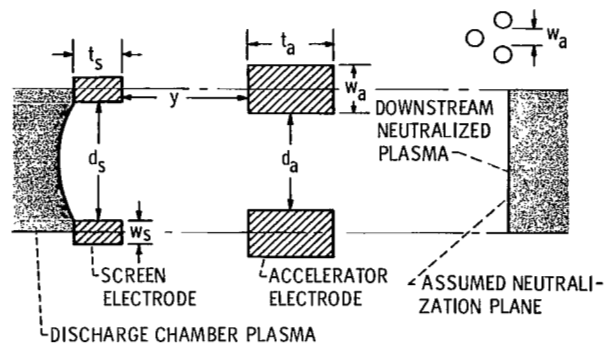
Figure 2. - Description of a single hole of a multihole two-grid accelerator system (refer to appendix A for symbol definitions).
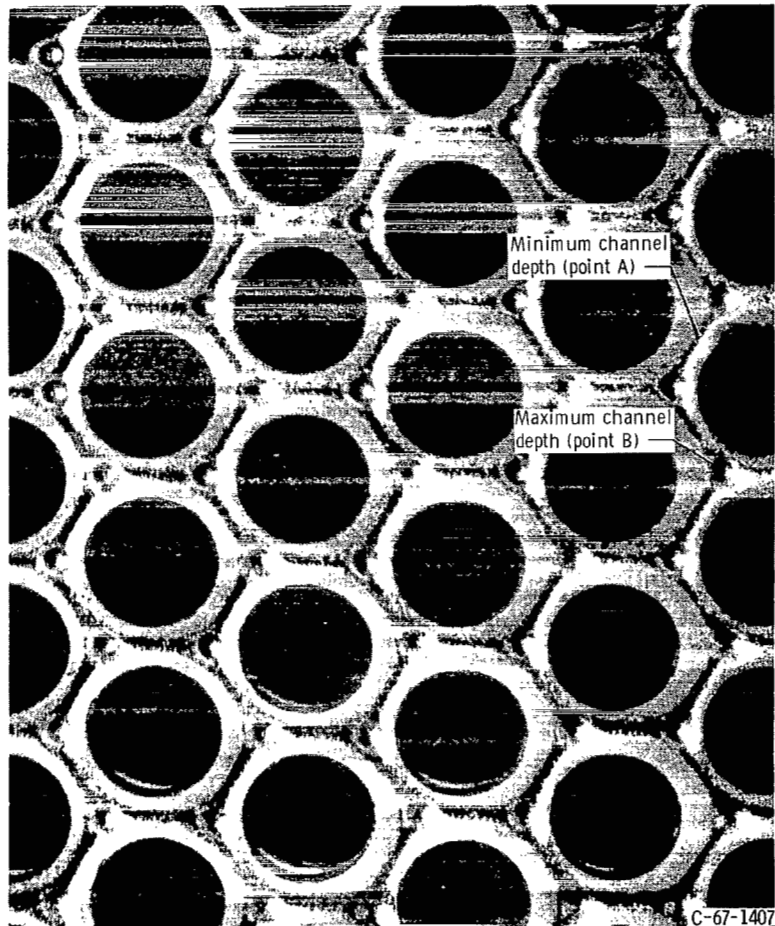
Figure 3. - Erosion pattern on downstream face of accelerator grid.

Parameter varied	Compare configurations-
Accelerator thickness, t_a	1, 3, and 5
Grid spacing, y	3 and 4
Accelerator hole diameter, d_a	2 and 3
Accelerator web thickness, w_a	2, 3, and 6
Fraction open area	3 and 6

(a) Configuration 1.

(b) Configuration 2.

(c) Configuration 3.

(d) Configuration 4.

(e) Configuration 5.
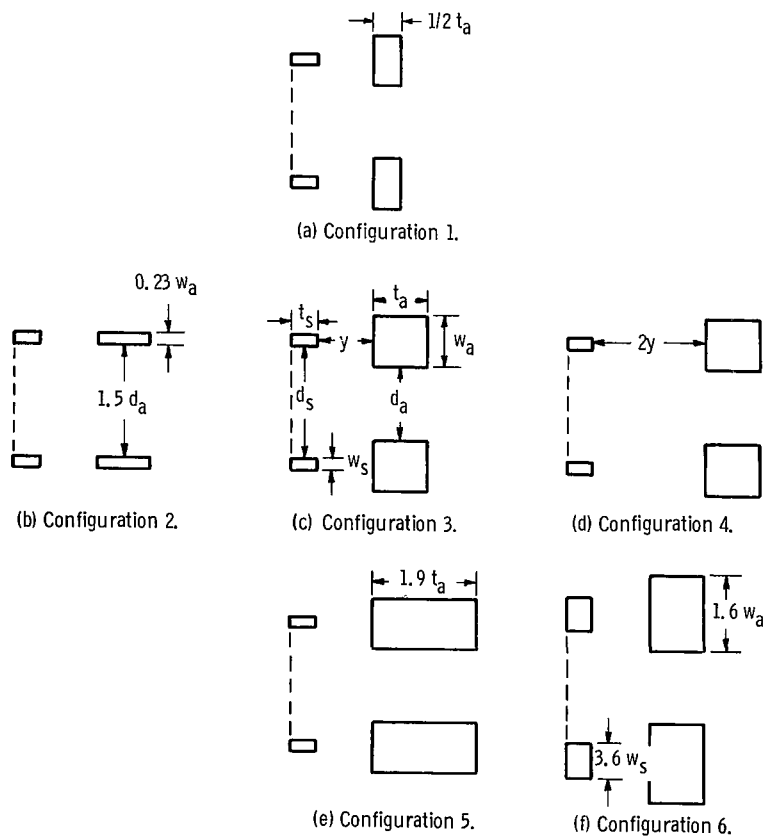
(f) Configuration 6.

Figure 4. – Description of configurations showing variation of geometrical parameters (refer to symbol list and table I).

(A) NARROW SCREEN.

(B) THICK SCREEN.
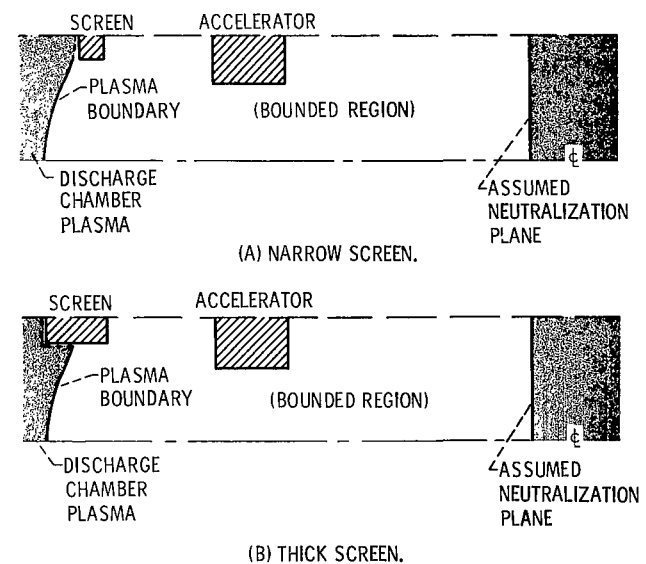
Figure 5. – Comparison of screen electrode thicknesses.
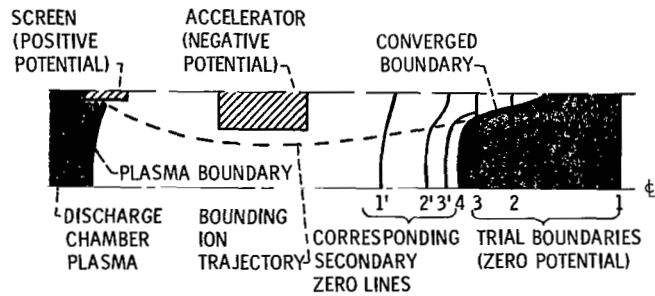
Figure 6. – Method for obtaining shape and location of downstream plasma boundary. (Cross section at point A, see fig. 3.)
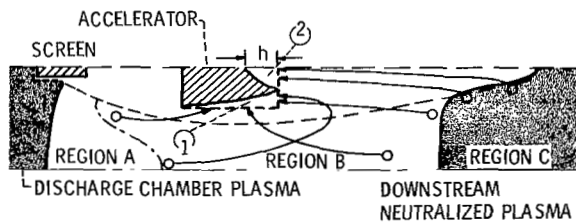
Figure 7. – Trajectories of typical charge-exchange ions, showing two distinct erosion regions (marked 1 and 2).
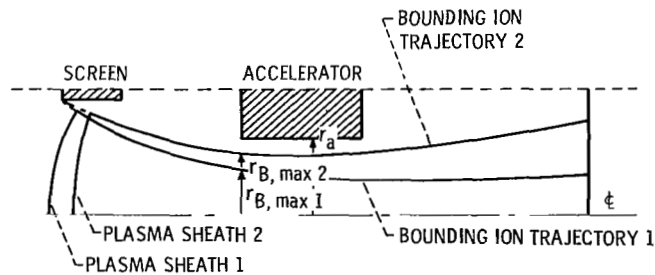
Figure 8. – Method for determining maximum current per hole $(J_{h,1} < J_{h,2})$.
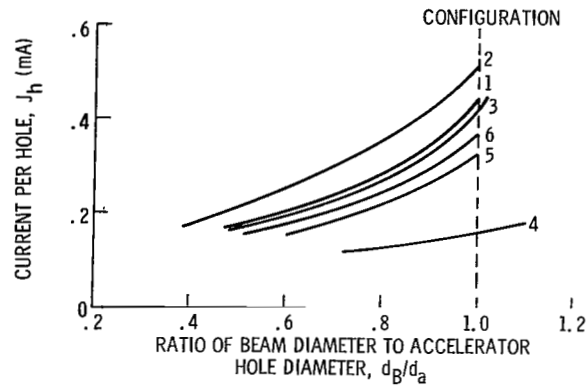
Figure 9. - Current per hole versus ratio of beam
diameter to accelerator hole diameter for six
configurations (see fig. 4).
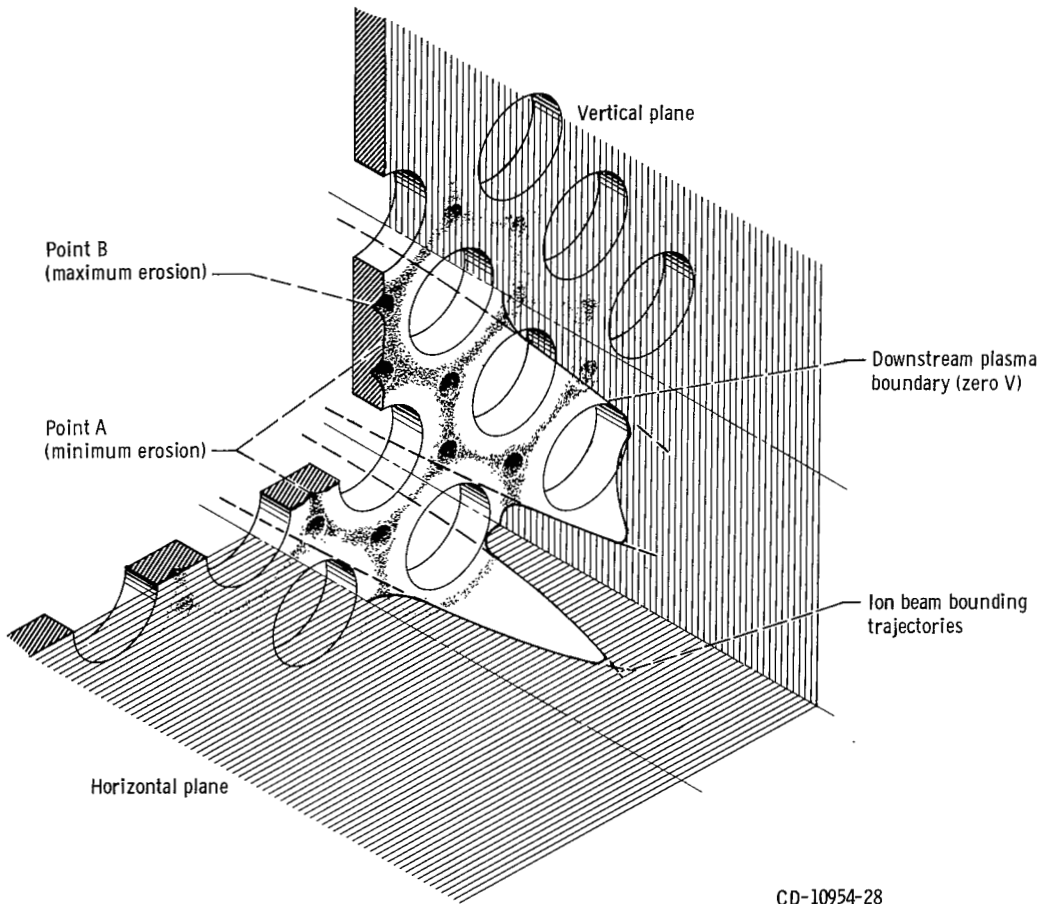
Figure 10. - Accelerator grid (at -2000 V) showing charge-exchange erosion patterns and downstream plasma boundary profiles.
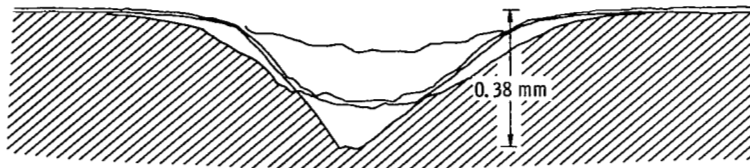
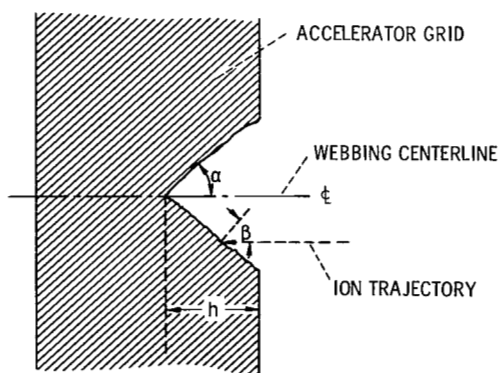Figure 11. – Typical grid erosion-pit cross sections as determined with a surface analyzer.

Figure 12. – Cross section through point A of acceler-
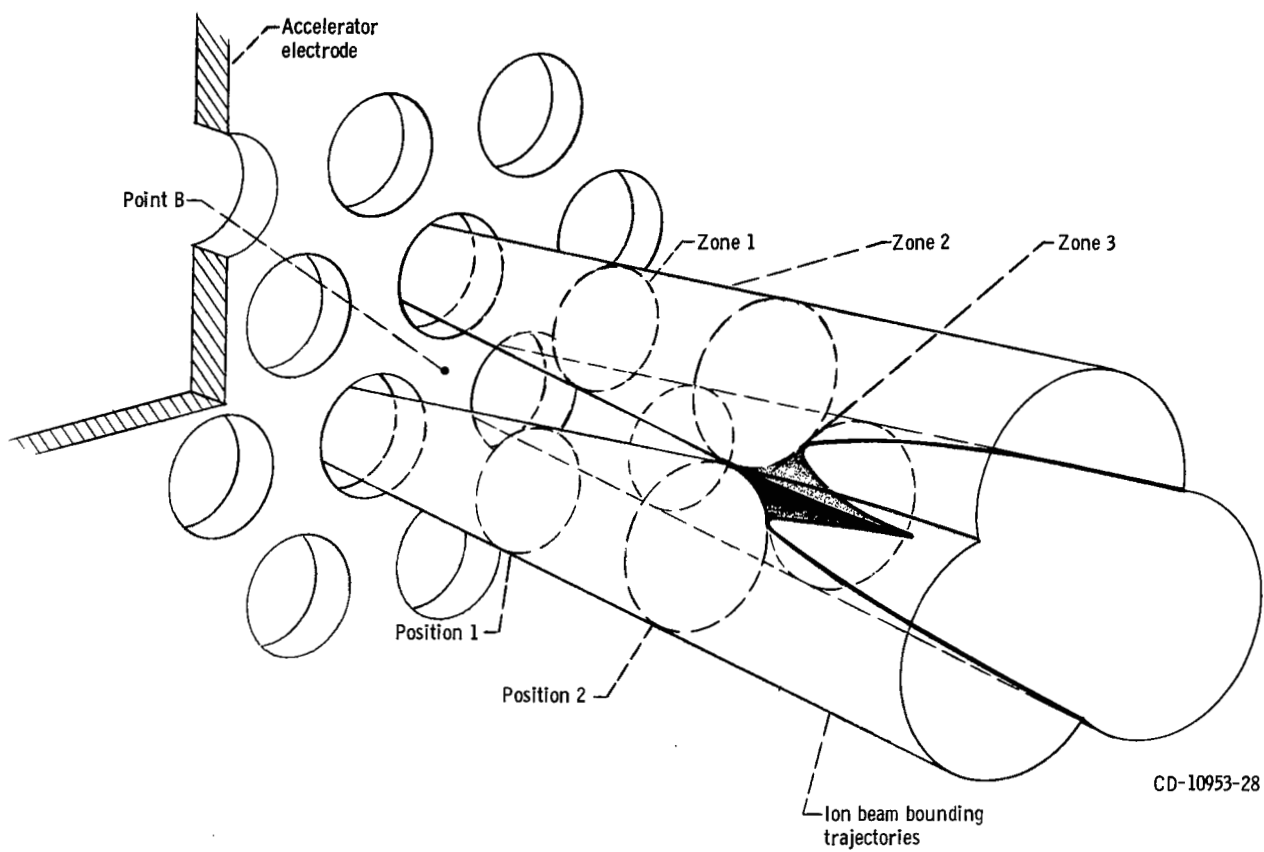ator grid, showing erosion on webbing centerline.

25

Figure 13. - Intersection of three ion beams. Beam divergence half-angle, 7°.

"The aeronautical and space activities of the United States shall be conducted so as to contribute ... to the expansion of human knowledge of phenomena in the atmosphere and space. The Administration shall provide for the widest practicable and appropriate dissemination of information concerning its activities and the results thereof."

— NATIONAL AERONAUTICS AND SPACE ACT OF 1958

NASA SCIENTIFIC AND TECHNICAL PUBLICATIONS

TECHNICAL REPORTS: Scientific and technical information considered important, complete, and a lasting contribution to existing knowledge.

TECHNICAL NOTES: Information less broad in scope but nevertheless of importance as a contribution to existing knowledge.

TECHNICAL MEMORANDUMS: Information receiving limited distribution because of preliminary data, security classification, or other reasons.

CONTRACTOR REPORTS: Scientific and technical information generated under a NASA contract or grant and considered an important contribution to existing knowledge.

TECHNICAL TRANSLATIONS: Information published in a foreign language considered to merit NASA distribution in English.

SPECIAL PUBLICATIONS: Information derived from or of value to NASA activities. Publications include conference proceedings, monographs, data compilations, handbooks, sourcebooks, and special bibliographies.

TECHNOLOGY UTILIZATION PUBLICATIONS: Information on technology used by NASA that may be of particular interest in commercial and other non-aerospace applications. Publications include Tech Briefs, Technology Utilization Reports and Technology Surveys.

Details on the availability of these publications may be obtained from:

SCIENTIFIC AND TECHNICAL INFORMATION OFFICE

NATIONAL AERONAUTICS AND SPACE ADMINISTRATION
Washington, D.C. 20546